ACCOUNTING FOR GRAIN BOUNDARY THICKNESS IN THE SUB-MICRON AND NANO SCALES

X. Zhang[1,2] and K.E. Aifantis[2,3]

[1]School of Civil Engineering and Mechanics, Huazhong University of Science and Technology, Wuhan 430074, China
[2]Lab of Mechanics and Materials, Aristotle University of Thessaloniki, Greece
[3]Physics, Michigan Technological University, USA

Abstract. Interfaces are explicitly accounted for, within gradient plasticity, by assigning a finite thickness to the interface or grain boundary and by differentiating between the constitutive properties of the "grain boundary" phase and the adjacent "bulk" phase. The present model is applied to consider the deformation of micro- and nano- crystalline materials under constant load or constant displacement rate conditions. The corresponding stress-strain curves exhibit serrations as observed experimentally during nanoindentation or microtensile tests: "plateaus" or "strain bursts" in the case of a constant load rate and "serrations" or "stress drops" in the case of a constant displacement rate. Such a genuine and routinely observed phenomenon when the deformation process is experimentally monitored by sufficiently sensitive devices in a variety of material classes is the main feature of the present contribution; a feature that has not been captured theoretically before with a simple analytical gradient plasticity model.

1. INTRODUCTION

In order to capture the effective response of materials that contain multiple interfaces, such as composites and nanomaterials, homogenization techniques [1-6] and molecular dynamics simulations [7-9] are commonly used. Another approach that has been successfully used is to consider the "composite" or the "nanopolycrystal" as a "mixture" of distinct superimposed and interconnected phases with different constitutive properties and balance laws assigned to each phase [10,11].

It is necessary, however, to develop a more rigorous formulation that can account explicitly for interfaces, as it has been well documented that the unique opto-electro-magnetic properties of nanomaterials are attributed to internal surfaces, such as grain boundaries and interfaces.

A theoretical formulation that can explicitly consider interfacial effects was presented in [5], the A-W model, according to which a separate interface energy was assigned to interfaces, within a gradient plasticity framework [5,6]. This approach has been successfully used to interpret the inverse Hall-Petch (H-P) behavior in nc-polycrystals [12]. The A-W model, however, treats grain boundaries as surfaces with zero thickness, which is not the case for grain boundaries in nanocrystalline materials. This assumption is removed here by allowing the grain boundary to possess a finite thickness and assigning to it different constitutive properties than those of the adjacent grains. Then, the stress-strain fields that continuously vary across the grain boundary are determined through the solution of a boundary value problem within a gradient plasticity framework to account for the dominating effect of plastic het-

Corresponding author: K.E. Aifantis, email: kaifanti@mtu.edu

Fig. 1. Geometric configuration of the unit cell model.

erogeneity and the associated development of high strain gradients.

The gradient plasticity theory adopted in our analysis is that essentially advanced by Aifantis [13,14], but within a variational formulation analogous to that used in the A-W model without allowing, however, for jumps across internal surfaces and corresponding interfacial energy penalty terms. Within such a framework, the solution of a standard mechanics boundary-value-problem for the assumed unit cell configuration is obtained analytically for both stress-controlled and strain-controlled loading conditions. Several new and interesting results are obtained in a straight forward manner. By confining attention to simple linear elastic-plastic behavior, it is possible to deduce explicit stress-strain relations which can exhibit discontinuities in the form of "plateaus" or "strain bursts" for stress (load) controlled tests ($d\sigma = 0$) and "serrations" or "stress drops" for strain (displacement) controlled tests ($d\varepsilon = 0$). Such stress-strain discontinuities are routinely recorded at the nanoscale when indenting near grain boundaries in nc-materials [15]. They have also been observed more frequently in micropillar compression [16]. Prior to this experimental evidence, such serrations were observed at macroscopic scales (by using appropriate "strain gage" devices) for various classes of materials: Al-Mg in the Portevin – Le Chatelier (PLC) regime, metallic glasses undergoing massive multiple shear band deformation, materials deforming by twinning. They were interpreted as the result of local deformation instabilities, which manifest themselves at the macroscopic level [13]. It is, thus, hoped that the present formulation may also be used for the aforementioned problems by replacing, for example, the "grain boundary" phase with the "shear band" phase.

The plan of the article is as follows: Section 2 provides the general variational formulation of the adopted unit cell model (the interface is identified as a grain boundary and it will be assumed as such throughout the paper). Section 3 derives the solution of the corresponding boundary value problem in the case that the grain boundary acts as a "hard" phase. This is the case of usual strain hardening behavior of conventional polycrystals where the grain boundaries act as obstacles to the intragrain dislocations. Stress–strain curves are obtained exhibiting "strain bursts" or "stress drops", as well as, size effects in accordance with the trends of normal Hall-Petch (H-P) behavior, *i.e.* smaller grain size associated with stiffer behavior. Section 4 contains analogous results, but for the case where the grain boundary acts as a "soft" phase. This is the case of nano-polycrystals (nc's) where the "interconnected grain boundary phase" is the carrier of plastic deformation, while the elastically deformed nanograins resist dislocation motion or nucleation within them. Stress–strain curves with "plateaus" or "serrations" are again obtained but, this time, size effects resembling the abnormal H-P relation are observed for nc's; *i.e.* below a critical grain size, smaller grain size is associated with a softening response. Finally, conclusions and prospects are listed in Section 5.

2. GRADIENT PLASTICITY CONSIDERING GRAIN BOUNDARY THICKNESS

As previously indicated, the unit cell model to be used is that of a 1-dimensional / two-phase configuration; *i.e.* a grain boundary phase of thickness L_{gb} is situated between two identical grains of size L_g. Both phases are deformed according to the gradient plasticity theory as first proposed by Aifantis [14] and later followed by others, including the aforementioned work of Fleck and Willis [4] and Aifantis and Willis [5] who provided a variational formulation of the theory and introduced interfacial energy effects (A–W model), which were shown to be in agreement with experimental data [17]. The configuration departs from the A–W model in the fact that the grain boundary is not just a surface of discontinuity but a region with finite width, which allows for a

smooth transition between the two adjacent grains that it connects. While such finite thickness considerations may not be necessary for describing macroscopic and microscopic behavior, it is of paramount importance for the description of sub-microscopic and nano configurations where internal length scales associated with the deformation of grain boundaries play a decisive role in determining the overall material behavior and the occurrence of size effects.

The energy functional for a gradient dependent continuum, in the deformation theory version of plasticity is assumed to be of the form

$$\Psi\left(\varepsilon,\varepsilon^{p}\right) = \int_{\Omega} U\left(\varepsilon,\varepsilon^{p},\nabla\varepsilon^{p}\right) d\Omega - \int_{\partial\Omega^{t}}\left(t^{0}u\right)dS - \int_{\partial\Omega^{m}}\left(m^{0}\varepsilon^{p}\right)dS. \tag{1}$$

$U(\varepsilon,\varepsilon^{p},\nabla\varepsilon^{p})$ is the elastoplastic potential, which accounts for a linear elastic term, and also the plastic potential V, which in the case of gradient plasticity depends on the plastic gradient as well

$$U\left(\varepsilon,\varepsilon^{p},\nabla\varepsilon^{p}\right) = \frac{1}{2}E\left(\varepsilon-\varepsilon^{p}\right)^{2} + V\left(\varepsilon^{p},\nabla\varepsilon^{p}\right). \tag{2}$$

The kinematic quantities $(u,\varepsilon,\varepsilon^{p},\nabla\varepsilon^{p})$ denote the displacement, total strain, plastic strain and plastic strain gradient, respectively; E is the elastic modulus; t^{0} is the "macroscopic" surface traction vector conjugate to u, and m^{0} is the "microscopic" surface traction tensor conjugate to ε^{p}. Ω denotes the sum of the three different domains making up the unit cell ($\Omega = \Omega_{g1} + \Omega_{g2} + \Omega_{gb}$), while $\partial\Omega^{t}$ and $\partial\Omega^{m}$ denote the parts of the external boundaries (in this case at $x = \pm[L_{gb} + L_{g}]$) where the traction t^{0} (or the displacement u) and the hypertraction m^{0} (or the plastic strain ε^{p}) are prescribed. (The subscript gb denotes the properties of the grain boundary, g1 the properties of grain 1 and g2 the properties of grain 2. Since grain 1 and grain 2 have the same material properties g1 = g2 = g.) The primary independent kinematic quantities in this model are the displacement u and the plastic strain ε^{p}; both are assumed to be continuous throughout the unit cell domain, along with their conjugate variables; this being the main departure from the A–W model where the higher order stress suffers a jump across the grain boundary and a corresponding surface energy penalty term appears in Eq. (1). The elastic strain is defined as usual by $\varepsilon^{e}=\varepsilon - \varepsilon^{p}$, while the total strain ε and the plastic strain gradient $\nabla\varepsilon^{p}$ are related to the independent kinematic quantities u and ε^{p} through the definitions

$$\varepsilon = \frac{du}{dx}, \quad \nabla\varepsilon^{p} = \frac{d\varepsilon^{p}}{dx}. \tag{3}$$

The respective conjugate variables to $(\varepsilon,\varepsilon^{p},\nabla\varepsilon^{p})$ are the total (Cauchy) stress σ, the internal (back) stress s, and the higher–order stress (hyperstress) τ. They are defined by the relations

$$\sigma = \frac{\partial U}{\partial\varepsilon} = E\left(\varepsilon-\varepsilon^{p}\right),$$

$$s = \frac{\partial U}{\partial\varepsilon^{p}} = -E\left(\varepsilon-\varepsilon^{p}\right) + \frac{\partial V}{\partial\varepsilon^{p}} = -\sigma + \frac{\partial V}{\partial\varepsilon^{p}}, \tag{4}$$

$$\tau = \frac{\partial U}{\partial\nabla\varepsilon^{p}} = \frac{\partial V}{\partial\nabla\varepsilon^{p}}.$$

It should be noted that the first two conjugate variable relations are also present in the classical case, but use of the plastic gradient $\nabla\varepsilon^{p}$ resulted in the definition of the higher–order stress. The requirement that the energy functional is minimized at equilibrium implies that the first variation of Eq. (1) has to be zero for all allowed variations of the kinematic quantities; hence, the "principle of virtual work" is defined as

$$\int_{\Omega}\left(\sigma\delta\varepsilon + s\delta\varepsilon^{p} + \tau\delta\nabla\varepsilon^{p}\right)d\Omega = \int_{\partial\Omega^{t}}\left(t^{0}\delta u\right)dS + \int_{\partial\Omega^{m}}\left(m^{0}\delta\varepsilon^{p}\right)dS. \tag{5}$$

Using the relationship between the kinematic variables Eq. (3), allows Eq. (5) to be re-written as

$$\int_{\Omega}\left(\sigma\delta\varepsilon_{,x} + s\delta\varepsilon^{p} + \tau\delta\varepsilon^{p}_{,x}\right)d\Omega = \int_{\partial\Omega^{t}}\left(t^{0}\delta u\right)dS + \int_{\partial\Omega^{m}}\left(m^{0}\delta\varepsilon^{p}\right)dS, \tag{6}$$

which, upon integration by parts and use of the divergence theorem, gives

$$\int_{\Omega}\left(-\sigma_{,x}\delta u + \left(s-\tau_{,x}\right)\delta\varepsilon^{p}\right)d\Omega + \int_{\Gamma}\left(\llbracket\sigma n\rrbracket\delta u + \llbracket\tau n\rrbracket\delta\varepsilon^{p}\right)d\Gamma = \int_{\partial\Omega^{t}}\left(t^{0} - \sigma n\right)\delta u\,dS + \int_{\partial\Omega^{m}}\left(m^{0} - \tau n\right)\delta\varepsilon^{p}\,dS, \tag{7}$$

where n denotes the unit outer normal to the unit cell external boundaries $\partial\Omega$ and the internal surfaces Γ. The corresponding jumps $\llbracket\sigma n\rrbracket$ and $\llbracket\tau n\rrbracket$ are defined by

$$\llbracket\sigma n\rrbracket = \sigma_{A}n_{A} + \sigma_{B}n_{B} = \left(\sigma_{A} - \sigma_{B}\right)n_{A} = \left(\sigma_{B} - \sigma_{A}\right)n_{B},$$

$$\llbracket\tau n\rrbracket = \tau_{A}n_{A} + \tau_{B}n_{B} = \left(\tau_{A} - \tau_{B}\right)n_{A} = \left(\tau_{B} - \tau_{A}\right)n_{B}. \tag{8}$$

According to the present formulation these jumps $[\![\sigma n]\!]$, $[\![\tau n]\!]$ are identically equal to zero. The indices A and B are used to denote the two subdomains which border the internal boundary Γ, with $n^A = -n^B$. It follows that in order for Eq. (7) to be identically satisfied for all allowed variations δu and $\delta \varepsilon^p$, the following field equations, outer boundary conditions, and internal boundary conditions hold:

$$\left. \begin{array}{c} \sigma_{,x} = 0 \\ s = \tau_{,x} \end{array} \right\} \text{ in subdomains } \Omega_i; \quad i = (g1, g2, gb), \quad (9)$$

$$\left. \begin{array}{c} [\![\sigma n]\!] = \sigma_i n_i + \sigma_{gb} n_{gb} = 0 \quad \text{or} \quad u = \overline{u} \\ [\![\tau n]\!] = \tau_i n_i + \tau_{gb} n_{gb} = 0 \quad \text{or} \quad \varepsilon^p = \overline{\varepsilon}^p \end{array} \right\} \quad (10)$$

across internal boundaries $\Gamma_{gb/bi}$; $i = (g1, g2)$,

$$\left. \begin{array}{c} \sigma n = t^0 \quad \text{or} \quad u = \overline{u} \\ \tau n = m^0 \quad \text{or} \quad \varepsilon^p = \overline{\varepsilon}^p \end{array} \right\} \text{ on outer surfaces}$$

$$\partial \Omega_i; \quad i = (g1, g2). \quad (11)$$

It is noted in particular that Eq. (10) suggests that the higher–order stress, τ, is continuous across internal boundaries when the two adjacent subdomains are in the plastic state.

To proceed further, constitutive equations must be defined for the plastic potential $V(\varepsilon^p, \nabla \varepsilon^p)$ for both the grain and the grain boundary phases. Motivated by [5], the following quadratic expression is adapted for V

$$V_i \left(\varepsilon_i^p, \varepsilon_{i,x}^p \right) = \sigma_i^{ys} \left| \varepsilon_i^p \right| + \frac{1}{2} \beta_i \left[\left(\varepsilon_i^p \right)^2 + l_i^2 \left(\varepsilon_{i,x}^p \right)^2 \right], \quad (12)$$

where σ_i^{ys} is the yield stress of the grain, β_i denotes the hardening modulus, and l_i is an internal length, accounting for the effect of strain gradients. The index $i = (gb, g)$ is used to denote the material properties in either the grain boundary phase or the grain interior. In particular, this form of V arises from a modification of the linear hardening rule for classical plasticity: the term $1/2\beta_i (\varepsilon_i^p)^2$ accounts for the effect of "statistically stored dislocations (SSD)" while the $1/2\beta_i l_i^p (\varepsilon_{i,x}^p)^2$ term accounts for the effect of "geometrical necessary dislocations (GND)". It is therefore seen that, unlike the plastic strain, the plastic strain gradient is not continuous across subdomains as $\beta_g l_g^2 \neq \beta_{gb} l_{gb}^2$.

With this definition for the plastic potential, Eq. (4) becomes

$$\sigma_i = E_i \left(\varepsilon_i - \varepsilon_i^p \right), \quad s_i = -\sigma_i + \sigma_i^{ys} + \beta_i \varepsilon_i^p,$$

$$\tau_i = \beta_i l_i^2 \varepsilon_{i,x}^p. \quad (13)$$

Table 1. Stages of deformation within submicron-scale domain.

	Stage 1	Stage 2	Stage 3
Grain interior	Elastic	Plastic	Plastic
Grain boundary	Elastic	Elastic	Plastic

Upon substitution of Eq. (13) into Eq. (9), we obtain the following differential equations

$$\frac{du_i}{dx} - \varepsilon_i^p - \frac{\overline{\sigma}}{E_i} = 0, \quad \frac{d^2 \varepsilon_i^p}{dx^2} - \frac{\varepsilon_i^p}{l_i^2} + \frac{\overline{\sigma} - \sigma_i^{ys}}{\beta_i l_i^2} = 0 \quad (14)$$

for the kinematic quantities u and ε^p. These are the governing equations for the assumed unit cell, which should be solved with the aid of appropriate boundary and continuity conditions in order to determine the deformation behavior and deduce stress–strain curves.

3. DEFORMATION BEHAVIOR FOR "STIFF" GRAIN BOUNDARIES

In this Section, the deformation behavior of the unit cell is considered when the grain boundary acts as an obstacle to intra-grain dislocation motion. This is the case for macroscopic and microscopic scales when the average grain size of the deforming polycrystal is of the order of microns and the yield stress of the grain boundary phase, σ_{gb}^{ys}, is higher than the grain interior yield stress, σ_g^{ys}. It is convenient then to consider the deformation of the unit cell by distinguishing among three different stages as shown in Table 1.

As these different stages are characterized by different boundary conditions, we solve the corresponding boundary value problem for each stage separately. Before doing so, however, it is useful to define the dimensionless variables below

$$l_g^* = \frac{L_g}{l_g}, \quad l_{gb}^* = \frac{L_{gb}}{l_{gb}}.$$

$$f_g = \frac{L_g}{L}, \quad f_{gb} = \frac{L_{gb}}{L}, \quad \widehat{f}_g^* = \frac{l_g}{L}, \quad \widehat{f}_{gb}^* = \frac{l_{gb}}{L}, \quad (15)$$

where $L = L_g + L_{gb}$.

3.1. The three-stage stress-strain curve

(i) *Stage One:* In the beginning of deformation for small applied stresses ($\overline{\sigma}$), both the grain bound-

ary and grain interior are in the elastic state. As there is no plastic strain ($\varepsilon_i^p = 0$) the displacement field is given by the expression

$$u_i = \frac{\overline{\sigma}}{E_i} x + C_i, \tag{16}$$

where $i = (g1, g2, gb)$ for both the grain interior phases $(g1, g2)$ and grain boundary phase (gb).

The constants (C_{g1}, C_{g2}, C_{gb}), are calculated by allowing the displacement to be fixed at zero at the surface of grain 2, while it remains continuous in going from one phase to the other; therefore the following boundary conditions are used

$$u_{g2}\left(-L_{gb} - L_g\right) = 0, \quad u_{g2}\left(-L_{gb}\right) = u_{gb}\left(-L_{gb}\right),$$
$$u_{g1}\left(L_{gb}\right) = u_{gb}\left(L_{gb}\right). \tag{17}$$

Finally, the stress-strain response is obtained by prescribing the displacement at the outer right hand side of the unit cell ($x = L_{gb} + L_g$) as

$$u_{g1}\left(L_{gb} + L_g\right) = 2\left(L_{gb} + L_g\right)\overline{\varepsilon}, \tag{18}$$

where $\overline{\varepsilon}$ denotes the overall macroscopic strain, associated with the applied stress . Solving Eq. (18) for the stress gives the overall stress–strain relation as

$$\overline{\sigma} = \frac{E_g E_{gb}\left(L_g + L_{gb}\right)}{E_g L_{gb} + E_{gb} L_g}\overline{\varepsilon}, \tag{19}$$

suggesting that the overall effective elastic modulus is identical to the Reuss modulus in composite materials theory, *i.e.*

$$\frac{1}{E_{Reuss}} = \frac{E_{gb} L_g + E_g L_{gb}}{E_g E_{gb}\left(L_g + L_{gb}\right)} = \frac{f_g}{E_g} + \frac{f_{gb}}{E_{gb}}, \tag{20}$$

where (f_g, f_{gb}) may be identical with the volume fractions of the grain interior and the grain boundary phases, respectively.

(ii) *Stage Two:*

Upon continuous deformation (e.g. by increasing the applied stress $\overline{\sigma}$) the grain interior will begin deforming plastically, while the grain boundary will remain elastic. Thus, the plastic strain at the grain boundary vanishes ($\varepsilon_{gb}^p = 0$) and the displacement is given by Eq. (16). The plastic strain in the grain interior is determined by solving the second differential equation in Eq. (14)

$$\varepsilon_i^p = \frac{\overline{\sigma} - \sigma_g^{ys}}{\beta_i} + A_i e^{x/l_i} + B_i e^{-x/l_i}, \tag{21}$$

which upon insertion into the first equation of Eq. (14) and subsequent integration yields the displacement expression

$$u_i = \frac{\overline{\sigma}}{E_i} x + \frac{\overline{\sigma} - \sigma_g^{ys}}{\beta_i} x + l_i A_i e^{x/l_i} - l_i B_i e^{-e/l_i} + C_i, \tag{22}$$

where $i = (g1, g2)$.

The constants $(A_{g1}, B_{g1}, A_{g2}, B_{g2})$ are determined by letting the plastic strain be zero on the grain boundary, since it is in the elastic regime, and by letting the higher order stress be zero on the external surface, according to Eq. (11), *i.e.*

$$\varepsilon_{g1}^p\left(L_{gb}\right) = 0, \quad \varepsilon_{g2}^p\left(-L_{gb}\right) = 0,$$
$$\tau_{g1}\left(L_{gb} + L_g\right) = 0, \quad \tau_{g2}\left(-L_{gb} - L_g\right) = 0 \tag{23}$$

while the values of (C_{g1}, C_{g2}, C_{gb}) are determined again through Eq. (17). Then Eq. (18) can be used to derive the corresponding stress-strain relationship

$$\overline{\sigma} = \sigma_g^{ys} +$$
$$\frac{\beta_g E_g E_{gb}\left(L_{gb} + L_g\right)}{\beta_g\left(E_{gb} L_g + E_g L_{gb}\right) + E_g E_{gb}\left[L_g - l_g \text{Tanh}\left(l_g^*\right)\right]} \times$$
$$\left(\overline{\varepsilon} - \overline{\varepsilon}_g^{ys}\right), \tag{24}$$

$\overline{\varepsilon}_g^{ys}$ denotes the critical strain at which the grain yields, and is given by the relation

$$\overline{\varepsilon}_g^{ys} = \frac{E_{gb} L_g + E_g L_{gb}}{E_g E_{gb}\left(L_g + L_{gb}\right)}\sigma_g^{ys} = \frac{\sigma_g^{ys}}{E_{Reuss}}. \tag{25}$$

The strain hardening rate (SHR) after the grain interior yields can be calculated through Eq. (24) as

$$\Theta_g = \frac{d\overline{\sigma}}{d\overline{\varepsilon}} = \frac{1}{\dfrac{1}{E_{Reuss}} + \dfrac{f_g}{\beta_g} + \dfrac{1}{L}\dfrac{1}{\beta_g}\dfrac{d\left(\Delta\tau_g\right)}{d\sigma}}, \tag{26}$$

where E_{Reuss} is the effective elastic modulus given by Eq. (20) and $\Delta\tau_g$ is the difference of the higher–order stress between the grain interior and the grain boundary, *i.e.*

$$\Delta\tau_g = \tau_{g1}\left(L_{gb} + L_g\right) - \tau_{g1}\left(L_{gb}\right) =$$
$$\tau_{g2}\left(-L_{gb}\right) - \tau_{g2}\left(-L_g - L_{gb}\right) =$$
$$l_g\left(\sigma_g^{ys} - \overline{\sigma}\right)\tanh\left(l_g^*\right). \tag{27}$$

In the limiting case of zero grain boundary thickness L_{gb}, Eq. (26) reduces to

$$\Theta_g = \frac{1}{\dfrac{1}{E_g} + \dfrac{1}{\beta_g} - \dfrac{1}{\beta_g}\dfrac{l_g}{L}\tanh\left(l_g^*\right)}, \tag{28}$$

which is exactly the expression obtained in [18] within the framework of the A–W model, which treated interfaces as surfaces discontinuity, without a thickness assigned to them.

If $L_g = l_g$, Eq. (28) degenerates further to the classical case

$$\Theta_g = \frac{1}{\dfrac{1}{E_g} + \dfrac{1}{\beta_g}}. \tag{29}$$

(iii) *Stage Three*: Upon continuous deformation (by increasing, for example, the applied stress) intra-grain dislocations can penetrate the grain boundary. As a result a strain burst or a stress drop occurs initially at a critical stress and strain ($\sigma_{gb}^{ys\Delta}$, $\overline{\varepsilon}_{gb}^{ys<}$), and then the whole system (both the grain and boundary) work hardens. Hence, both the grain interior and the grain boundary deform plastically according to Eq. (21), while the displacement expression is given by Eq. (22), with $i = (g1, g2, gb)$ in both equations.

The constants of integration ($A_{g1}, B_{g1}, A_{g2}, B_{g2}, A_{gb}, B_{gb}$) are now determined by letting the higher–order stress and plastic strain to be continuous throughout the whole system, and again the higher order stress is set equal to zero at the outer surface,

$$\tau_{g1}\left(L_{gb} + L_g\right) = 0, \quad \tau_{g2}\left(-L_{gb} - L_g\right) = 0,$$
$$\varepsilon_{g1}^{p}\left(L_{gb}\right) = \varepsilon_{gb}^{p}\left(L_{gb}\right), \quad \tau_{g1}\left(L_{gb}\right) = \tau_{gb}\left(L_{gb}\right),$$
$$\varepsilon_{g2}^{p}\left(-L_{gb}\right) = \varepsilon_{gb}^{p}\left(-L_{gb}\right), \quad \tau_{g2}\left(-L_{gb}\right) = \tau_{gb}\left(-L_{gb}\right). \tag{30}$$

Similarly as before the (C_{g1}, C_{g2}, C_{gb}) are determined by Eq. (17), and then the stress-strain relationship is calculated through Eq. (18) as

$$\overline{\sigma} = \sigma_{gb}^{ys*} + \left[\frac{\beta_g \beta_{gb}\left(L_g E_{gb} + L_{gb} E_g\right) + E_g E_{gb}\left(L_g \beta_{gb} + L_{gb}\beta_g\right)}{\beta_g \beta_{gb} E_g E_{gb} L} + \right.$$
$$\left. \left(\frac{1}{\beta_g} - \frac{1}{\beta_{gb}}\right)\frac{1}{L}\frac{\left(\beta_g - \beta_{gb}\right)l_g l_{gb}\tanh\left(l_g^*\right)\tanh\left(l_{gb}^*\right)}{\left(\beta_g l_g \tanh\left(l_g^*\right) + \beta_{gb} l_{gb}\tanh\left(l_{gb}^*\right)\right)} \right]^{-1} \left(\overline{\varepsilon} - \overline{\varepsilon}_{gb}^{ys*}\right). \tag{31}$$

Where (σ_{gb}^{ys*}, $\overline{\varepsilon}_{gb}^{ys*}$) represent the initiation of work hardening of this deformation stage. For the strain burst case, σ_{gb}^{ys*} is the grain boundary stress ($\sigma_{gb}^{ys\Delta}$) and $\overline{\varepsilon}_{gb}^{ys*} = \overline{\varepsilon}_{gb}^{ys<}$ which is the strain at which the strain bursts ends.

$$\overline{\varepsilon}_{gb}^{ys>} = \frac{f_g}{E_g} + \frac{f_{gb}}{E_{gb}}\sigma_g^{ys} + \left[\frac{f_g}{E_g} + \frac{f_{gb}}{E_{gb}} + \frac{f_g}{\beta_g} + \frac{\left(\beta_g - \beta_{gb}\right)l_g l_{gb}\tanh\left(l_g^*\right)\tanh\left(l_{gb}^*\right)}{\beta_g L\left(\beta_g l_g \tanh\left(l_g^*\right) + \beta_{gb} l_{gb}\tanh\left(l_{gb}^*\right)\right)}\right]\left(\sigma_{gb}^{ys\Delta} - \sigma_g^{ys}\right). \tag{32}$$

For the stress drop case, $\overline{\varepsilon}_{gb}^{ys*}$ is the strain at which the grain boundry yields ($\overline{\varepsilon}_{gb}^{ys<}$) and σ_{gb}^{ys*} is the stress after the stress drop $\sigma_{gb}^{ys\nabla}$,

$$\sigma_{gb}^{ys\nabla} = \frac{\overline{\varepsilon}_g^{ys}}{\dfrac{f_g}{E_g} + \dfrac{f_{gb}}{E_{gb}}} + \frac{\overline{\varepsilon}_{gb}^{ys<} - \overline{\varepsilon}_g^{ys}}{\dfrac{f_g}{E_g} + \dfrac{f_{gb}}{E_{gb}} + \dfrac{f_g}{\beta_g} + \dfrac{\left(\beta_g - \beta_{gb}\right)l_g l_{gb}\tanh\left(l_g^*\right)\tanh\left(l_{gb}^*\right)}{\beta_g L\left(\beta_g l_g \tanh\left(l_g^*\right) + \beta_{gb} l_{gb}\tanh\left(l_{gb}^*\right)\right)}}. \tag{33}$$

The strain hardening rate (SHR), after the grain boundary yields, is denoted by Θ_{gb} and can be calculated through Eq. (31) as

$$\Theta_{gb} = \frac{d\overline{\sigma}}{d\overline{\varepsilon}} = \frac{1}{\dfrac{1}{E_{\text{Reuss}}} + \dfrac{1}{\beta_{\text{Reuss}}} + \dfrac{1}{L}\left(\dfrac{1}{\beta_g}\dfrac{d\left(\Delta\tau_g\right)}{d\sigma} + \dfrac{1}{\beta_{gb}}\dfrac{d\left(\Delta\tau_{gb}\right)}{d\sigma}\right)}, \tag{34}$$

where E_{Reuss} is the effective elastic modulus defined as before

$$\frac{1}{E_{\text{Reuss}}} = \frac{E_{gb}L_g + E_g L_{gb}}{E_g E_{gb}\left(L_g + L_{gb}\right)} = \frac{f_g}{E_g} + \frac{f_{gb}}{E_{gb}}. \tag{35}$$

(a) Strain burst under stress control   (b) Stress drop under strain control
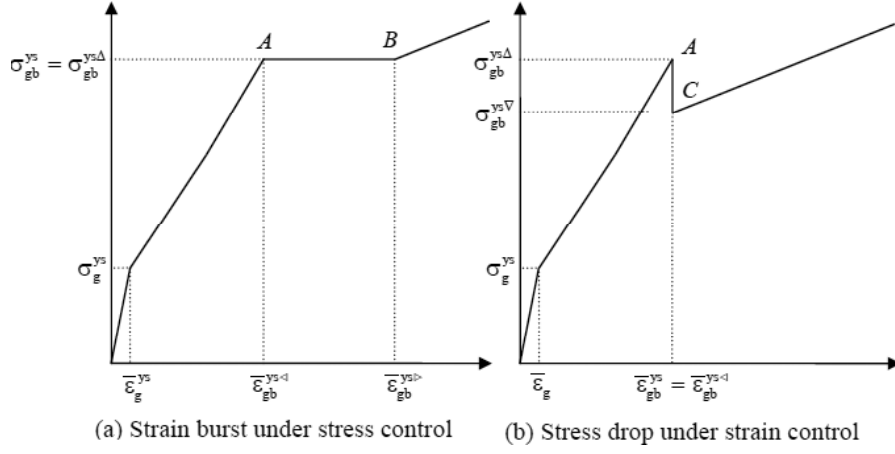
Fig. 2. Stress-strain relationship for different loading conditions: (a) Strain burst after grain boundary yielding under stress control. (b) Stress drop after grain boundary yielding under strain control.

β_{Reuss} denotes an analogous effective hardening modulus defined in a similar way by

$$\frac{1}{\beta_{\text{Reuss}}} = \frac{\beta_{gb}L_g + \beta_g L_{gb}}{\beta_g \beta_{gb} \left(L_g + L_{gb}\right)} = \frac{f_g}{\beta_g} + \frac{f_{gb}}{\beta_{gb}}. \tag{36}$$

$\Delta\tau_g$ denotes the difference of the higher order stress in the grain interior, *i.e.*

$$\Delta\tau_g = \tau_{g1}\left(L_{gb} + L_g\right) - \tau_{g1}\left(L_{gb}\right) = \tau_{g2}\left(-L_{gb}\right) - \tau_{g2}\left(-L_g - L_{gb}\right) =$$
$$-\frac{\left[\beta_{gb}\left(\overline{\sigma} - \sigma_g^{ys}\right) + \beta_g\left(-\overline{\sigma} + \sigma_{db}^{ys}\right)\right]l_g l_{gb} \tanh\left(l_g^*\right)\tanh\left(l_{gb}^*\right)}{\left[\beta_g l_g \tanh\left(l_g^*\right) + \beta_{gb} l_{gb} \tanh\left(l_{gb}^*\right)\right]} \tag{37}$$

and $\Delta\tau_{gb}$ denotes the difference of the higher order stress in the grain boundary, *i.e.*

$$\Delta\tau_{gb} = \tau_{gb}\left(L_{gb}\right) - \tau_{gb}\left(0\right) = \tau_{gb}\left(0\right) - \tau_{gb}\left(-L_{gb}\right) =$$
$$\frac{\left[\beta_{gb}\left(\overline{\sigma} - \sigma_g^{ys}\right) + \beta_g\left(-\overline{\sigma} + \sigma_{db}^{ys}\right)\right]l_g l_{gb} \tanh\left(l_g^*\right)\tanh\left(l_{gb}^*\right)}{\left[\beta_g l_g \tanh\left(l_g^*\right) + \beta_{gb} l_{gb} \tanh\left(l_{gb}^*\right)\right]}. \tag{38}$$

It turns out that Eq. (34) degenerates to Eq. (24) of reference [18] when the thickness of the grain boundary is vanishingly small ($L_{gb} = 0$) and it further degenerates to the classical case when $L_g = l_g$; i.e. when the effect of the strain gradient and higher order stress is ignored.

3.2. Discontinuities in the stress-strain curves

A new feature that can be deduced from the above analysis is the possibility of interpreting theoretically various "discontinuities" in the stress-strain curves that have been observed experimentally in the form of "strain bursts" or "stress drops" for stress/load controlled or strain/displacement controlled tests. Such discontinuities may occur during the transition from stage 2 to stage 3. Both the strain bursts and stress drops occur when the stress attains the critical value $\sigma_{gb}^{ys\Delta}$ or when the strain attains the critical value $\overline{\varepsilon}_{gb}^{ys<}$. When the test is stress-controlled, a strain burst will occur at $\sigma_{gb}^{ys\Delta}$, and the burst will have a length ($\overline{\varepsilon}_{gb}^{ys>}$ - $\overline{\varepsilon}_{gb}^{ys<}$), while when the test is strain controlled a stress drop will occur at $\overline{\varepsilon}_{gb}^{ys<}$ and the observed stress difference will be ($\sigma_{gb}^{ys\Delta}$ - $\sigma_{gb}^{ys\nabla}$). Therefore, V_{gb} in Eq. (12) is defined separately for these two cases

$$V_{gb}\left(\varepsilon_{gb}^p, \varepsilon_{gb,x}^p\right) = \sigma_{gb}^{ys\Delta}\left|\varepsilon^p\right| + \frac{1}{2}\beta_{gb}\left[\left(\varepsilon_{gb}^p\right)^2 + l_{gb}^2\left(\varepsilon_{gb,x}^p\right)^2\right] \tag{39}$$

for stress-controlled tests, and by

$$V_{gb}\left(\varepsilon_{gb}^{p},\varepsilon_{gb,x}^{p}\right) = \sigma_{gb}^{ys\nabla}\left|\varepsilon^{p}\right| + \frac{1}{2}\beta_{gb}\left[\left(\varepsilon_{gb}^{p}\right)^{2} + l_{gb}^{2}\left(\varepsilon_{gb,x}^{p}\right)^{2}\right] \tag{40}$$

for strain-controlled tests.

The corresponding full stress-strain curves for the two types of loading are depicted qualitatively in Fig. 2 and analytically presented below as follows:

(i) For stress-controlled tests: The overall stress ($\overline{\sigma}$) – strain ($\overline{\varepsilon}$) graph is given by the expressions

$$\overline{\varepsilon} = \begin{cases} \dfrac{E_g L_{gb} + E_{gb} L_g}{E_g E_{gb} L}\overline{\sigma}; \;\; 0 < \overline{\sigma} < \sigma_g^{ys} \\[3mm] \overline{\varepsilon}_g + \dfrac{\beta_g\left(E_{gb}L_g + E_g L_{gb}\right) + E_g E_{gb}\left(L_g - l_g \tanh\left(l_g^{*}\right)\right)}{\beta_g E_g E_{gb} L}\left(\overline{\sigma} - \sigma_g^{ys}\right); \;\; \sigma_g^{ys} < \overline{\sigma} < \sigma_{gb}^{ys\Delta} \\[3mm] \overline{\varepsilon}_{gb}^{ys<} \rightarrow \overline{\varepsilon}_{gb}^{ys>}; \;\; \overline{\sigma} = \sigma_{gb}^{ys\Delta} \\[3mm] \overline{\varepsilon}_{gb}^{ys>} + \left\{\dfrac{\beta_g\beta_{gb}\left(L_g E_{gb} + L_{gb} E_g\right) + E_g E_{gb}\left(L_g\beta_{gb} + L_{gb}\beta_g\right)}{\beta_g\beta_{gb}E_g E_{gb}L} + \right. \\[3mm] \left. \dfrac{1}{L}\times\left(\dfrac{1}{\beta_g} - \dfrac{1}{\beta_{gb}}\right)\dfrac{\left(\beta_g - \beta_{gb}\right)l_g l_{gb}\tanh\left(l_g^{*}\right)\tanh\left(l_{gb}^{*}\right)}{\left(\beta_g l_g \tanh\left(l_g^{*}\right) + \beta_{gb} l_{gb}\tanh\left(l_{gb}^{*}\right)\right)}\right\}\left(\overline{\sigma} - \sigma_{gb}^{ys\Delta}\right); \;\; \overline{\sigma} > \sigma_{gb}^{ys\Delta} \end{cases} , \tag{41}$$

where

$$\overline{\varepsilon}_g^{ys} = \frac{1}{E_{\text{Reuss}}}\sigma_g^{ys},$$

$$\overline{\varepsilon}_{gb}^{ys<} = \frac{1}{E_{\text{Reuss}}}\sigma_g^{ys} + \frac{1}{\Theta_g}\left(\sigma_{gb}^{ys\Delta} - \sigma_g^{ys}\right), \tag{42}$$

$$\overline{\varepsilon}_{gb}^{ys>} = \frac{1}{E_{\text{Reuss}}}\sigma_g^{ys} + \frac{1}{\Theta_{g/gb}}\left(\sigma_{gb}^{ys\Delta} - \sigma_g^{ys}\right)$$

with

$$E_{\text{Reuss}} = \frac{1}{\dfrac{f_g}{E_g} + \dfrac{f_{gb}}{E_{gb}}},$$

$$\Theta_g = \frac{1}{\dfrac{f_g}{E_g} + \dfrac{f_{gb}}{E_{gb}} + \dfrac{f_g}{\beta_g} - \dfrac{1}{\beta_g}\dfrac{l_g}{L}\tanh\left(l_g^{*}\right)}, \tag{43}$$

$$\Theta_{g/gb} = \frac{1}{\dfrac{f_g}{E_g} + \dfrac{f_{gb}}{E_{gb}} + \dfrac{f_g}{\beta_g} + \dfrac{\left(\beta_g - \beta_{gb}\right)l_g l_{gb}\tanh\left(l_g^{*}\right)\tanh\left(l_{gb}^{*}\right)}{\beta_g L\left(\beta_g l_g \tanh\left(l_g^{*}\right) + \beta_{gb} l_{gb}\tanh\left(l_{gb}^{*}\right)\right)}}.$$

(ii) For strain-controlled tests: The overall stress ($\overline{\sigma}$) – strain ($\overline{\varepsilon}$) graph is given by the expressions

$$\overline{\sigma} = \begin{cases} \dfrac{E_g E_{gb} L}{E_g L_{gb} + E_{gb} L_g} \, \overline{\varepsilon}; \ \ 0 < \overline{\varepsilon} < \overline{\varepsilon}_g^{ys} \\[3mm] \sigma_g^{ys} + \dfrac{\beta_g E_g E_{gb} L}{\beta_g \left(E_{gb} L_g + E_g L_{gb}\right) + E_g E_{gb}\left(L_g - l_g \tanh\left(l_g^*\right)\right)}\left(\overline{\varepsilon} - \overline{\varepsilon}_g^{ys}\right); \ \ \overline{\varepsilon}_g^{ys} < \overline{\varepsilon} < \overline{\varepsilon}_{gb}^{ys<} \\[3mm] \sigma_{gb}^{ys\Delta} \rightarrow \sigma_{gb}^{ys\nabla}; \ \ \overline{\varepsilon} = \overline{\varepsilon}_{gb}^{ys<} \\[3mm] \sigma_{gb}^{ys\nabla} + \left\{ \dfrac{\beta_g \beta_{gb}\left(L_g E_{gb} + L_{gb} E_g\right) + E_g E_{gb}\left(L_g \beta_{gb} + L_{gb}\beta_g\right)}{\beta_g \beta_{gb} E_g E_{gb} L} + \right. \\[3mm] \left. \dfrac{1}{L} \times \left(\dfrac{1}{\beta_g} - \dfrac{1}{\beta_{gb}}\right)\dfrac{\left(\beta_g - \beta_{gb}\right)l_g l_{gb}\tanh\left(l_g^*\right)\tanh\left(l_{gb}^*\right)}{\left(\beta_g l_g \tanh\left(l_g^*\right) + \beta_{gb} l_{gb}\tanh\left(l_{gb}^*\right)\right)} \right\}^{-1}\left(\overline{\varepsilon} - \overline{\varepsilon}_{gb}^{ys<}\right); \ \ \overline{\varepsilon} > \overline{\varepsilon}_{gb}^{ys<} \end{cases} , \tag{44}$$

where

$$\sigma_g^{ys} = E_{\text{Reuss}} \, \overline{\varepsilon}_g^{ys},$$
$$\sigma_{gb}^{ys\Delta} = E_{\text{Reuss}} \, \overline{\varepsilon}_g^{ys} + \Theta_g \left(\overline{\varepsilon}_{gb}^{ys<} - \overline{\varepsilon}_g^{ys}\right), \tag{45}$$
$$\sigma_{gb}^{ys\nabla} = E_{\text{Reuss}} \, \overline{\varepsilon}_g^{ys} + \Theta_{g/gb} \left(\overline{\varepsilon}_{gb}^{ys<} - \overline{\varepsilon}_g^{ys}\right)$$

with $(E_{\text{Reuss}}, \Theta_g, \Theta_{g/gb})$ given as before.

It should be noted that in Eq. (41) the stain is given in terms of the stress as the experiment was stress controlled. In plotting, however, these expressions they were re-written in terms of the strain. Having, thus, derived the full stress-strain graphs for both stress-controlled and strain controlled tests we can compute the "strain burst" and "stress drop" magnitudes by an elaborate, but straightforward calculation. The details of this calculation will be included in a forthcoming article [19] as they are not necessary for the subsequent physical discussion. Nevertheless, we list the central relationships for these quantities for the completeness of the presentation. In fact, it can be shown without difficulty that the "strain burst" $\Delta\overline{\varepsilon}$ (for the condition $d\overline{\sigma} = 0$) is given by

$$\Delta\overline{\varepsilon} = \overline{\varepsilon}_{gb}^{>} - \overline{\varepsilon}_{gb}^{<} = \left[\dfrac{1}{\Theta_{g/gb}} - \dfrac{1}{\Theta_g}\right]\left(\sigma_{gb}^{ys\Delta} - \sigma_g^{ys}\right) = \dfrac{l_g \tanh\left(l_g^*\right)}{L_g + L_{gb}}\dfrac{l_g \tanh\left(l_g^*\right) + l_{gb}\tanh\left(l_{gb}^*\right)}{\beta_g l_g \tanh\left(l_g^*\right) + \beta_{gb} l_{gb}\tanh\left(l_{gb}^*\right)}\left(\sigma_{gb}^{ys\Delta} - \sigma_g^{ys}\right). \tag{46}$$

It also turns out that an alternative expression for the magnitude of the "strain burst" $\Delta\overline{\varepsilon}$ can be derived in terms of the discontinuity of the hyperstress $[\![\tau_g]\!]$ or $[\![\tau_{gb}]\!]$ as follows

$$\Delta\overline{\varepsilon} = \dfrac{\left|[\![\tau]\!]_g\right|}{\beta_g l_g \tanh\left(l_g^*\right)}\left(\hat{f}_g^* \tanh\left(l_g^*\right) + \hat{f}_{gb}^* \tanh\left(l_{gb}^*\right)\right) = \dfrac{\left|[\![\tau]\!]_{gb}\right|}{\beta_{gb} l_{gb}\tanh\left(l_{gb}^*\right)}\left(\hat{f}_g^* \tanh\left(l_g^*\right) + \hat{f}_{gb}^* \tanh\left(l_{gb}^*\right)\right). \tag{47}$$

In a similar way we can compute the magnitude of the "stress drop" $\Delta\overline{\sigma}$ (for the condition $d\overline{\varepsilon}$) is given by

$$\Delta\sigma = \sigma_{gb}^{ys\Delta} - \sigma_{gb}^{ys\nabla} = \left(\Theta_g - \Theta_{g/gb}\right)\left(\overline{\varepsilon}_{gb}^{ys<} - \overline{\varepsilon}_g^{ys}\right) \tag{48}$$

and, thus, the following interesting relation is obtained

$$\dfrac{\Delta\overline{\sigma}}{\Delta\overline{\varepsilon}} = \dfrac{\left(\Theta_g - \Theta_{g/gb}\right)\left(\overline{\varepsilon}_{gb}^{ys<} - \overline{\varepsilon}_g^{ys}\right)}{\left(\dfrac{1}{\Theta_{g/gb}} - \dfrac{1}{\Theta_g}\right)\left(\sigma_{gb}^{ys\Delta} - \sigma_g^{ys}\right)} = \Theta_{g/gb}. \tag{49}$$

Summarizing the above results, we have shown that in going from stage 2 to stage 3, of Table 1, discontinuities in the stress-strain plot can take place through either a "strain burst" or "stress drop", as the grain boundary phase yields.

In particular, the following two cases, depending on the loading conditions can occur:

(i) If the experiment is stress controlled, once the grain boundary yields, dislocations will be transmitted across and therefore an avalanche of strain bursts will be present in the stress-strain plot. For this case Eq. (41)$_1$ is plotted until the grain yield stress is reached (σ_g^{ys}); then Eq. (41)$_2$ takes over and is plotted until the grain boundary yields ($\sigma_{gb}^{ys\Delta}$), at which point the strain burst occurs and the constant stress is given by Eq. (41)$_3$. Once the dislocation transmittance across the boundary is completed the material continues to work harden according to Eq. (41)$_4$. This is shown in Fig. 2a.

(ii) If the experiment is strain controlled, upon grain boundary yielding, the stress required for continuous plastic flow will drop, as the hardening that was induced by the impenetrable grain boundary does not exist anymore. This suggests that Eq. (44)$_1$ is plotted until the grain yield strain is reached ($\overline{\varepsilon}_g^{ys}$); after which work hardening takes place in the grain and the response is defined by Eq. (44)$_2$. At a critical strain the grain boundary yields ($\overline{\varepsilon}_{gb}^{ys<}$), and therefore, does not act as a barrier to plastic flow; hence, the stress required for continuous deformation drops and a stress drop takes place as indicated by Eq. (44)$_3$. With continuing deformation the whole material deforms in a hardening manner according to Eq. (44)$_4$, as shown in Fig. 2b.

Both of the above-mentioned stress-strain responses are possible based on the loading conditions and their physical interpretation is as follows:

In Fig. 2a, initially the response is purely elastic and the "traditional knee" is obtained when the grains yield. Then the grains deform in a hardening manner and the grain boundary acts as a barrier to dislocation motion, leading to multiple dislocation pile-ups. Once, however, a critical stress is reached the grain boundary begins deforming plastically, allowing for dislocation transference to occur from both grains, leading to a perfectly plastic response and a corresponding strain burst in the stress-strain plot. Such experimental evidence has been observed in the compression of micropillars [16] and a more precise comparison with the existing experimental data is currently being undertaken.

In Fig. 2b, however, it is seen that it is also possible to have a stress drop take place, instead of a strain burst, once the grain boundary yields. The underlying physical mechanism for this is that initially, as long as the grain boundary is stiff, it acts as an obstacle to dislocation motion and contributes to a hardening response of the material. Once, however, the grain boundary yields the overall stress required to continue plastic deformation drops. This is similar to the hardness drop observed in nanoindentation data once the grain and grain boundary yields [18]; in fact Isozaki [20] attributed the effect of stress drops to grain boundary sliding, which may be viewed as a type of grain boundary yielding. Furthermore, discrete dynamic dislocations have captured the occurrence of stress drops in heterogeneous plastic flow, which is confined to a few deformation bands [21]. In particular, they predicted that when dislocations are distributed heterogeneously, they interact with each other to form tangles and junctions and pinning points; at a critical state of stress, they can bow out of these entangled structures leading to dislocation bursts and stress drops. In the present three-phase model this pinning takes place as the dislocations pile up at the grain boundary (as long as it remains elastic) and once it yields the dislocations can penetrate it, bow through it, leading to a stress drop. Stress drops have also been noted extensively in the literature for cases where dislocations were pinned on impurity or solute atoms [22] but in the present case the only pinning agent was the grain boundary.

3.3. Stress-strain curves and size effects

In order to obtain a comparative understanding of how the stress-strain response depends on the grain size, four different grain sizes are considered. The aforementioned formulation allows for the grains to yield initially and then the grain boundary. Such a mechanism is true for the submicron-scale and, therefore, the grain sizes are taken as L_g= 0.05, 0.1, 0.15, and 0.2 μm. The internal length of the grain (l_g) has to be smaller or equal to the grain size and is therefore set equal to the smallest L_g considered, *i.e.* l_g= 0.05 μm. The grain boundary thickness is kept constant at 2 nm (L_{gb}= 1 nm), and, therefore, its internal length is set equal to the grain boundary half thickness (l_g= 1 nm).

Copper is of the most studied metals, and therefore its material properties will be used. Therefore, The mechanical constants in the Cu grains are E_g= 120 GPa, σ_g^{ys} = 70 MPa, and β_g= 1.695 GPa (cal-
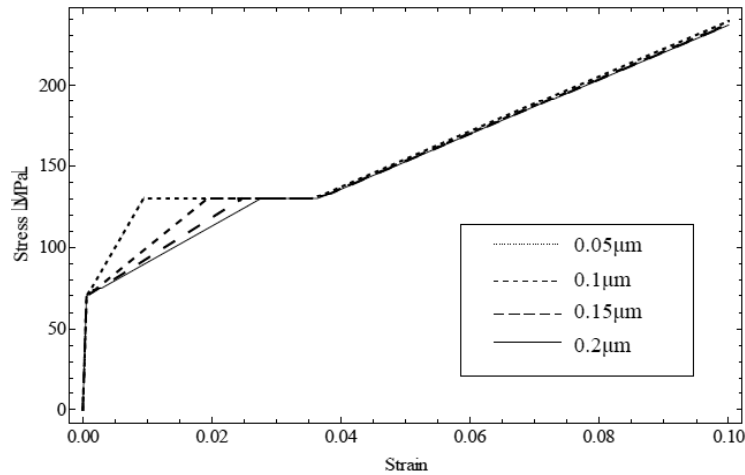
Fig. 3. Stress-strain response for Cu submicron-bicrystal under stress control loading.
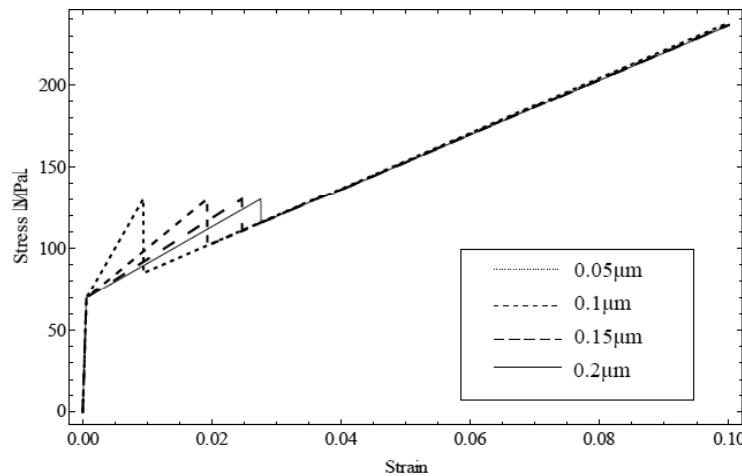
Fig. 4. Stress-strain response for Cu submicron-bicrystal under strain control loading.

culated from [23]). The parameters in the Cu grain boundary are defined according to [7] as E_{gb} = 75.9 GPa, $\sigma_{gb}^{ys\Delta}$ = 130 MPa, β_{gb} = 3 GPa. Inserting, therefore, these parameters and grain sizes in Eqs. (1) and (4), respectively, gives the resulting stress-strain response for this system for both types of loading as shown in Figs. 3 and 4.

In both Figs. 3 and 4 it is seeing that as the grain size decreases, the flow stress required for continuous plastic deformation increases, which is what is expected for microstructured materials, according to the Hall-Petch relationship. It is interesting to note that a size effect in the stress-strain response is present only in the region where grain boundary yielding takes place. The size effects collapse afterwards, indicating that plastic deformation is governed by the grains, and since the grain yield stress is taken to be independent of grain size, the overall plastic flow appears the same for all grain sizes considered. According to experimental data, however, both in single crystals [16] and polycrys-

tals [24] the grain yield stress is dependent on the grain size. So Figs. 3 and 4 can be re-plotted by varying the yield stress for each grain size according to Table 2.

As expected, significant size effects are now obtained in Figs. 5 and 6, since the yield stress of the grain interior which dominates deformation, is allowed to vary depending on the grain size.

4. DEFORMATION BEHAVIOR FOR "SOFT" GRAIN BOUNDARIES

Although nanomaterials are promising in new industrial application, their use is compromised by their lower ductility limiting their practical use [25-27]. Although Hall-Petch predicts that as the grain size decreases the hardness increases, there exists a critical grain size below which nanocrystalline materials become softer. It's, therefore, important to understand the underlying mechanisms dominating deformation at the nanoscale. It is believed that grain
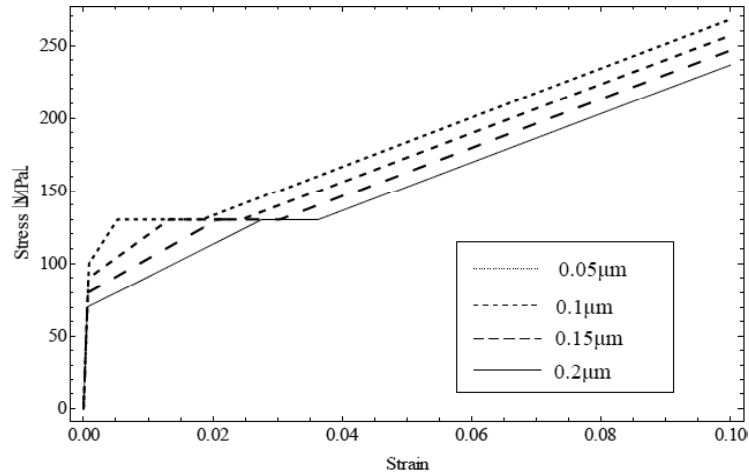
Fig. 5. Stress-strain response for Cu submicron bicrystal under stress control, when the grain yield stress is dependent on grain size.
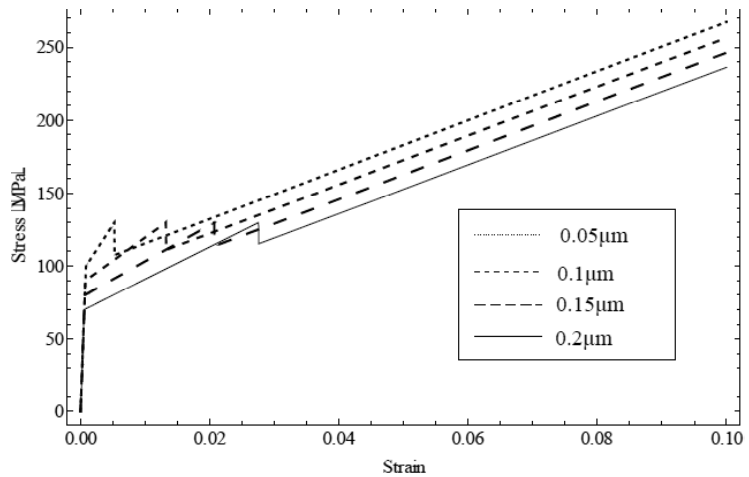
Fig. 6. Stress-strain response for Cu submicron bicrystal under strain control, when the grain yield stress is dependent on grain size.

boundary sliding, grain boundary diffusion, lattice dislocation slip, twin deformation, Coble creep, and triple junction diffusion creep are in competition during plastic flow in nc-polycrystals [25,28].

GB dislocations and dipoles of wedge disclinations, which are produced during grain boundary sliding and migration through the triple junctions, create stress concentrations that initiate nanocracks and induce early failure of the nanocrystal [29,30]. Such disclication stresses can be released through grain boundary diffusion, and a theoretical model developed by Ovid'ko [29] shows that good ductility can be achieved by optimizing the grain boundary

sliding and diffusion process. When deformation is accumulated in the grain boundary region [25], instead of the grain interior, the abnormal Hall-Petch phenomenon on the hardness is observed. Deformation in nc-polycrystals, therefore, occurs mainly in the grain boundary phase which is interconnected and evolves plastically with the nanograins acting as hard inclusions. In nanocrystals, therefore, grain

Table 2. Yield stress dependence on grain size.

$L_{g,}$ (mm)	0.2	0.15	0.1	0.05
$\sigma_{g,}^{ys}$ (MPa)	70	80	90	100

Table 3. Stages of deformation within nano-scale domain.

	Stage 1	Stage 2	Stage 3
Grain interior	Elastic	Elastic	Plastic
Grain boundary	Elastic	Plastic	Plastic

boundaries are "softer" than the grains, as they initiate and govern deformation. Thus, at the nanoscale, the grain boundary phase will yield before the grain interior phase; hence, the yield stress of the grain boundary, σ_{gb}^{ys} is smaller than that of the grain, σ_g^{ys}.

In trying to model the deformation of nanocrystals, we may consider three stages of deformation, and the formulation presented in Section 2 is still valid, but now yielding occurs in a different order as shown in Table 3.

(i) Stage 1: For initial elastic deformation we have the same situation as in Section 3 and the overall stress-strain response is given by the relation

$$\overline{\sigma} = E_{\text{Reuss}}\,\overline{\varepsilon}; \quad E_{\text{Reuss}} = \frac{E_g E_{gb}\left(L_g + L_{gb}\right)}{E_{gb}L_g + E_g L_{gb}}, \tag{50}$$

where E_{Reuss} is the effective elastic modulus of the Reuss composite material.

(ii) *Stage 2*: With continuous deformation the grain boundary will begin deforming plastically, while the grain interior will remain elastic. The plastic strain and displacement in the grain boundary is determined as before through the relationships

$$\varepsilon_{gb}^p = \frac{\overline{\sigma} - \sigma_{gb}^{ys}}{\beta_{gb}} + A_{gb}e^{x/l_{gb}} + B_{gb}e^{-x/l_{gb}},$$

$$u_{gb} = \frac{\overline{\sigma}}{E_{gb}}x + \frac{\overline{\sigma} - \sigma_{gb}^{ys}}{\beta_{gb}}x + l_{gb}A_{gb}e^{x/l_{gb}} - l_{gb}B_{gb}e^{-x/l_{gb}} + C_{gb}. \tag{51}$$

As there is no plastic strain in the grain interior, the displacement in the grain interior phase is again given by Eq. (16), while the constants (A_{gb}, B_{gb}) are determined by allowing the plastic strain to be continuous throughout the whole domain and therefore,

$$\varepsilon_{g1}^p\left(L_{gb}\right) = 0, \quad \varepsilon_{g2}^p\left(-L_{gb}\right) = 0. \tag{52}$$

The constants (C_{g1}, C_{g2}, C_{gb}) are also determined by an analogous way as in the previous section and, thus, the overall stress-strain response for Stage 2 is given by the relation

$$\overline{\sigma} = \sigma_{gb}^{ys} + \frac{\beta_{gb}E_b E_{gb}\left(L_g + L_{gb}\right)}{\beta_{gb}\left(E_g L_{gb} + E_{gb}L_g\right) + E_g E_{gb}\left(L_{gb} - l_{gb}\tanh\left(l_{gb}^*\right)\right)}\left(\overline{\varepsilon} - \overline{\varepsilon}_{gb}\right), \tag{53}$$

where $\overline{\varepsilon}_{gb}$ is the critical strain at which the grain boundary yields and is defined by

$$\overline{\varepsilon}_{gb} = \frac{E_{gb}L_g + E_g L_{gb}}{E_g E_{gb}\left(L_g + L_{gb}\right)}\sigma_{gb}^{ys}. \tag{54}$$

(ii) Stage 3: Upon continuous deformation dislocations may be emitted into the grain, which can then begin deforming plastically. At the onset of this transition ($\sigma_{gb}^{ys\Delta}$, $\overline{\varepsilon}_{gb}^{ys<}$) a strain burst or a stress drop will occur initially, and then the whole system (both the grain and grain boundary) work hardens. By employing similar arguments as in the previous section the overall stress-strain response for this final deformation stage is determined by the relation

$$\overline{\sigma} = \sigma_g^{ys*} + \left[\frac{\beta_g\beta_{gb}\left(L_g E_{gb} + L_{gb}E_g\right) + E_g E_{gb}\left(L_g\beta_{gb} + L_{gb}\beta_g\right)}{\beta_g\beta_{gb}E_g E_{gb}L} + \right.$$

$$\left.\left(\frac{1}{\beta_g} - \frac{1}{\beta_{gb}}\right)\frac{1}{L}\frac{\left(\beta_{gb} - \beta_g\right)l_g l_{gb}\tanh\left(l_g^*\right)\tanh\left(l_{gb}^*\right)}{\left(\beta_g l_g \tanh\left(l_g^*\right) + \beta_{gb}l_{gb}\tanh\left(l_{gb}^*\right)\right)}\right]^{-1}\left(\overline{\varepsilon} - \overline{\varepsilon}_g^{ys*}\right). \tag{55}$$

where (σ_g^{ys*}, $\overline{\varepsilon}_g^{ys*}$) represent the initiation of work hardening after grain interior yielding. For the strain burst case, σ_g^{ys*} is the stress $\sigma_g^{ys\Delta}$ and $\overline{\varepsilon}_g^{ys*}$ is the strain after the strain burst and is equal to $\overline{\varepsilon}_g^{ys>}$,

$$\overline{\varepsilon}_g^{ys>} = \left(\frac{f_g}{E_g} + \frac{f_{gb}}{E_{gb}}\right)\sigma_g^{ys} + \left[\frac{f_g}{E_g} + \frac{f_{gb}}{E_{gb}} + \frac{f_{gb}}{\beta_{gb}} + \frac{(\beta_{gb} - \beta_g)l_g l_{gb} \tanh(l_g^*)\tanh(l_{gb}^*)}{\beta_g L(\beta_g l_g \tanh(l_g^*) + \beta_{gb} l_{gb} \tanh(l_{gb}^*))}\right](\sigma_g^{ys\Delta} - \sigma_{gb}^{ys}). \tag{56}$$

For the stress drop case, $\overline{\varepsilon}_g^{ys*}$ is the strain $\overline{\varepsilon}_g^{ys<}$ and σ_g^{ys*} is the stress after the stress drop and is equal to

$$\sigma_g^{ys\nabla} = \frac{\overline{\varepsilon}_g^{ys}}{\frac{f_g}{E_g} + \frac{f_{gb}}{E_{gb}}} + \frac{\overline{\varepsilon}_{gb}^{ys<} - \overline{\varepsilon}_g^{ys}}{\frac{f_g}{E_g} + \frac{f_{gb}}{E_{gb}} + \frac{f_{gb}}{\beta_{gb}} + \frac{(\beta_{gb} - \beta_g)l_g l_{gb}\tanh(l_g^*)\tanh(l_{gb}^*)}{\beta_{gb}L(\beta_g l_g \tanh(l_g^*) + \beta_{gb} l_{gb}\tanh(l_{gb}^*))}}. \tag{57}$$

Although in ultrafine nanomaterials, it is most likely that the grain interior will never deform, for illustrative purposes here it will be taken that eventually it can.

In summary, the stress-strain response is given in Eqs. (58) and (61).

(i) For stress-controlled tests: The overall stress ($\overline{\sigma}$) – strain ($\overline{\varepsilon}$) graph is given by the expressions

$$\overline{\varepsilon} = \begin{cases} \dfrac{E_g L_{gb} + E_{gb}L_g}{E_g E_{gb}L}\,\overline{\sigma}; \quad 0 < \overline{\sigma} < \sigma_{gb}^{ys} \\[4mm] \overline{\varepsilon}_{gb} + \dfrac{\beta_{gb}(E_{gb}L_g + E_g L_{gb}) + E_g E_{gb}(L_{gb} - l_{gb}\tanh(l_{gb}^*))}{\beta_{gb}E_g E_{gb}L}(\overline{\sigma} - \sigma_{gb}^{ys}); \quad \sigma_{gb}^{ys} < \overline{\sigma} < \sigma_g^{ys\Delta} \\[4mm] \overline{\varepsilon}_g^{ys<} \to \overline{\varepsilon}_g^{ys>}; \quad \overline{\sigma} = \sigma_g^{ys\Delta} \\[4mm] \overline{\varepsilon}_g^{ys>} + \left\{\dfrac{\beta_g \beta_{gb}(L_g E_{gb} + L_{gb}E_g) + E_g E_{gb}(L_g \beta_{gb} + L_{gb}\beta_g)}{\beta_g \beta_{gb}E_g E_{gb}L} + \right. \\[4mm] \left. \dfrac{1}{L}\times\left(\dfrac{1}{\beta_{gb}} - \dfrac{1}{\beta_g}\right)\dfrac{(\beta_{gb} - \beta_g)l_g l_{gb}\tanh(l_g^*)\tanh(l_{gb}^*)}{(\beta_g l_g \tanh(l_g^*) + \beta_{gb}l_{gb}\tanh(l_{gb}^*))}\right\}(\overline{\sigma} - \sigma_g^{ys\Delta}); \quad \overline{\sigma} > \sigma_g^{ys\Delta} \end{cases}, \tag{58}$$

where

$$\overline{\varepsilon}_{gb}^{ys} = \frac{1}{E_{\text{Reuss}}}\sigma_{gb}^{ys},$$

$$\overline{\varepsilon}_g^{ys<} = \frac{1}{E_{\text{Reuss}}}\sigma_{gb}^{ys} + \frac{1}{\Theta_{gb}}(\sigma_g^{ys\Delta} - \sigma_{gb}^{ys}), \tag{59}$$

$$\overline{\varepsilon}_g^{ys>} = \frac{1}{E_{\text{Reuss}}}\sigma_{gb}^{ys} + \frac{1}{\Theta_{g/gb}}(\sigma_g^{ys\Delta} - \sigma_{gb}^{ys})$$

with

$$E_{\text{Reuss}} = \frac{1}{\dfrac{f_g}{E_g} + \dfrac{f_{gb}}{E_{gb}}},$$

$$\Theta_{gb} = \frac{1}{\dfrac{f_g}{E_g} + \dfrac{f_{gb}}{E_{gb}} + \dfrac{f_{gb}}{\beta_{gb}} - \dfrac{1}{\beta_{gb}}\dfrac{l_{gb}}{L}\tanh(l_{gb}^*)},$$

$$\tag{60}$$

$$\Theta_{g/gb} = \frac{1}{\dfrac{f_g}{E_g} + \dfrac{f_{gb}}{E_{gb}} + \dfrac{f_{gb}}{\beta_{gb}} + \dfrac{(\beta_{gb} - \beta_g)l_g l_{gb}\tanh(l_g^*)\tanh(l_{gb}^*)}{\beta_{gb}L(\beta_g l_g \tanh(l_g^*) + \beta_{gb}l_{gb}\tanh(l_{gb}^*))}}.$$
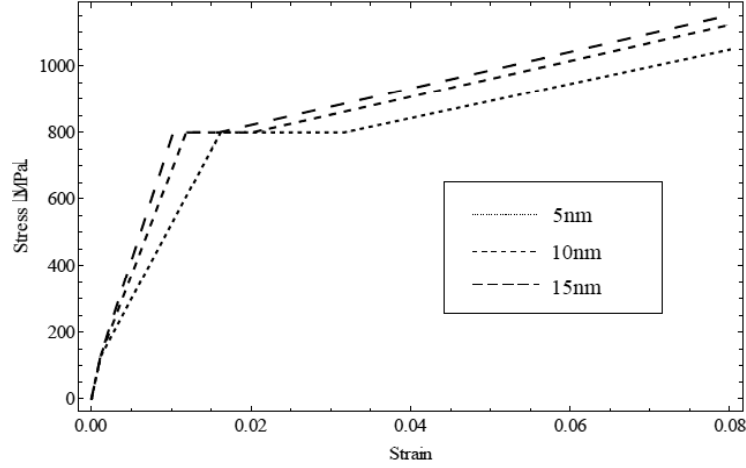
Fig. 7. Stress-strain response for Cu nanocrystalline under stress control loading.

(ii) For strain-controlled tests: The overall stress ($\bar{\sigma}$) – strain ($\bar{\varepsilon}$) graph is given by the expressions

$$\bar{\sigma} = \begin{cases} \dfrac{E_g E_{gb} L}{E_g L_{gb} + E_{gb} L_g} \bar{\varepsilon}; \ \ 0 < \bar{\varepsilon} < \bar{\varepsilon}_{gb}^{ys} \\[4mm] \sigma_{gb}^{ys} + \dfrac{\beta_{gb} E_g E_{gb} L}{\beta_{gb}\left(E_{gb} L_g + E_g L_{gb}\right) + E_g E_{gb}\left(L_{gb} - l_{gb} \tanh\left(l_{gb}^{*}\right)\right)}\left(\bar{\varepsilon} - \bar{\varepsilon}_{gb}^{ys}\right); \ \ \bar{\varepsilon}_{gb}^{ys} < \bar{\varepsilon} < \bar{\varepsilon}_g^{ys<} \\[4mm] \sigma_g^{ys\Delta} \rightarrow \sigma_g^{ys\nabla}; \ \ \bar{\varepsilon} = \bar{\varepsilon}_g^{ys<} \\[4mm] \sigma_g^{ys\nabla} + \left\{ \dfrac{\beta_g \beta_{gb}\left(L_g E_{gb} + L_{gb} E_g\right) + E_g E_{gb}\left(L_g \beta_{gb} + L_{gb}\beta_g\right)}{\beta_g \beta_{gb} E_g E_{gb} L} + \right. \\[4mm] \left. \dfrac{1}{L} \times \left(\dfrac{1}{\beta_{gb}} - \dfrac{1}{\beta_g}\right) \dfrac{\left(\beta_{gb} - \beta_g\right) l_g l_{gb} \tanh\left(l_g^{*}\right)\tanh\left(l_{gb}^{*}\right)}{\left(\beta_g l_g \tanh\left(l_g^{*}\right) + \beta_{gb} l_{gb} \tanh\left(l_{gb}^{*}\right)\right)}\right\}^{-1}\left(\bar{\varepsilon} - \bar{\varepsilon}_g^{ys<}\right); \ \ \bar{\varepsilon} > \bar{\varepsilon}_g^{ys<} \end{cases} , \tag{61}$$

where

$$\sigma_{gb}^{ys} = E_{\text{Reuss}} \bar{\varepsilon}_{gb}^{ys},$$
$$\sigma_g^{ys\Delta} = E_{\text{Reuss}} \bar{\varepsilon}_{gb}^{ys} + \Theta_{gb}\left(\bar{\varepsilon}_g^{ys<} - \bar{\varepsilon}_{gb}^{ys}\right), \tag{62}$$
$$\sigma_g^{ys\nabla} = E_{\text{Reuss}} \bar{\varepsilon}_{gb}^{ys} + \Theta_{g/gb}\left(\bar{\varepsilon}_g^{ys<} - \bar{\varepsilon}_{gb}^{ys}\right)$$

with ($E_{\text{Reuss}}, \Theta_g, \Theta_{g/gb}$) given as before.

It is noted that Eqs. (58) and (61) are identical to Eqs. (41) and (44) if we interchange the subscripts as $g \leftrightarrow gb$, since now the order of yielding in the unit cell is reversed.

4.1. Stress-strain curves and size effects

As for the sub-micron scale case, discontinuities occur in the stress-strain plot after the second phase yields, which in this case is the grain. Therefore, qualitative plots similar to those of Fig. 2 are expected in this nanoscale case as well. Only now the strain bursts or stress drops occur once the grain yields.

For the present case the material parameters should meet the following requirements: $E_{gb} < E_g$ and $\beta_{gb} < \beta_g$, while the grain size is taken to have a nanometer length. In particular, Eqs. (58) and (61) are plotted, in Figs. 7 and 8, for the following parameters:
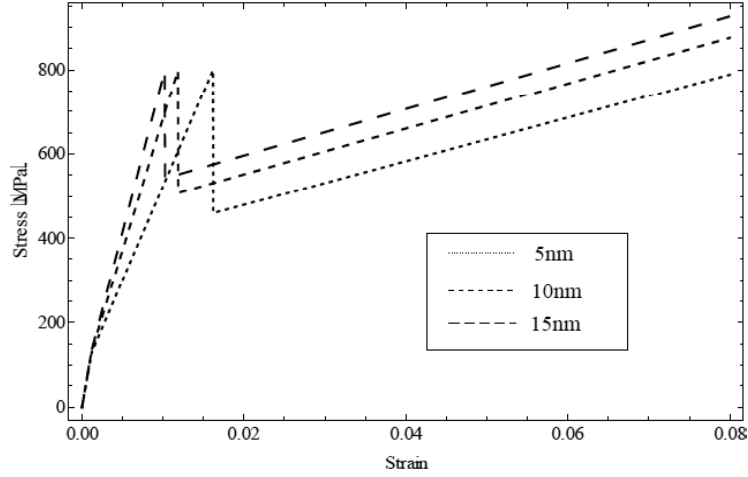
Fig. 8. Stress-strain response for Cu nanocrystalline under strain control loading.
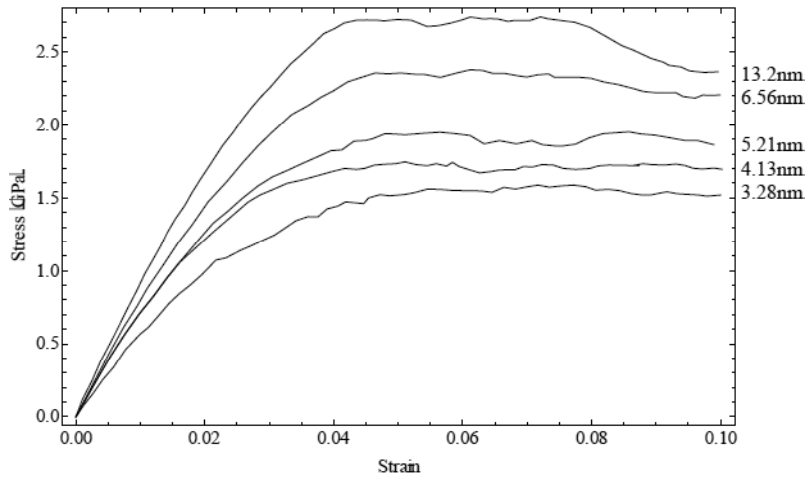
Fig. 9. Atomistic simulations on copper [31].

$\sigma_g^{ys\Delta} = 800\,\text{MPa}, E_g = 120\,\text{GPa}, \beta_g = 6\,\text{GPa},$

$l_g = 5\,\text{nm}, L_g = (5,10,15)\,\text{nm},$

$\sigma_{gb}^{ys} = 130\,\text{MPa}, E_{gb} = 75.9\,\text{GPa}, \beta_{gb} = 3\,\text{GPa},$

$l_{gb} = 1\,\text{nm}, L_{gb} = 1\,\text{mm},$

It is seen in Figs. 7 and 8 that the size effects are always significant, despite the fact that the grain yield stress is kept the same for all sizes considered. It is interesting to note that for this nanostructured case an inverse dependence of the flow stress on the grain size is observed; as the grain size decreases the plastic flow required for continuous deformation decreases, as well. This is opposite than the expected increase of the flow stress as the grain size decreased, observed in Figs. 3-6 for the sub-micron case. Although experiments documenting the flow stress as a function of grain size for nanomaterials are very delicate to design

and perform, it is indeed anticipated that nanomaterials below a certain grain size exhibit a size effect as shown in Figs. 7 and 8. In fact atomistic simulations [31] as shown in Fig. 9, on very fine grained Cu exhibit the same size dependence as the present formulation suggests.

5. CONCLUSIONS

In the present study gradient plasticity was employed to explicitly account for grain boundaries, by treating them as a separate phase with a finite thickness, and allowing them, therefore, to follow their own yield behavior. The unit cell model consisted therefore of two phases, the grain phase and the grain boundary phase. The novel feature of treating grain boundaries in this manner is that strain bursts and stress drops are explicitly predicted for in the stress-strain response, depending on the loading conditions. In particular, for stress controlled

loading a strain burst was observed once the harder phase yielded, whereas a stress drop was observed under strain controlled loading. Depending on the scale of the microstructure, the softer phase, which yields first, was taken to be either the grain (for the submicron case) or the grain boundary (for the nano case). In particular, it was noted that letting the grain boundary yield before the grain, which is the case for nanocrystals, the flow stress decreased as the grain size decreased. To the authors knowledge such an "inverse" size effect in the overall stress-strain response, has not been predicted previously from a theoretical or experimental point of view. It has, however, been anticipated by simulation results. A more detailed comparison between the present gradient plasticity model and experimental data of nanomaterials (interpretation of the "anomalous" Hall-Petch dependence of the hardness on the grain size) is currently being undertaken.

ACKNOWLEDGEMENTS

REFERENCES

[1] D. Talbot and J. Willis // *Proceedings: Mathematical and Physical Sciences* **447** (1930) 365.

[2] P. Castaneda // *Journal of the Mechanics and Physics of Solids* **39(1)** (1991) 45.

[3] P. Castaneda and P. Suquet // *Nonlinear composites. Advances in applied mechanics* **34** (1998) 171.

[4] N. Fleck and J. Willis // *Journal of the Mechanics and Physics of Solids* **52(8)** 2004 1855.

[5] K.E. Aifantis and J.R. Willis // *Journal of the Mechanics and Physics of Solids* **53(5)** (2005) 1047.

[6] K.E. Aifantis and J.R. Willis // *Mechanics of Materials* **38(8-10)** (2006) 702.

[7] B. Jiang and G.J. Weng // *Journal of the Mechanics and Physics of Solids* **52(5)** (2004) 1125.

[8] G. Weng // *Rev. Adv. Mater. Sci* **19** (2009) 41.

[9] L. Capolungo, M. Cherkaoui and J. Qu // *International Journal of Plasticity* **23(4)** (2007) 561.

[10] J. Carsley *et al.* // *Nanostructured Materials* **5(4)** (1995) 441.

[11] D.A. Konstantinidis and E.C. Aifantis // *Nanostructured Materials* **10(7)** (1998) 1111.

[12] R.K. Abu Al-Rub, G.Z. Voyiadjis and E.C. Aifantis // *International Journal of Materials & Product Technology* **34(1-2)** (2009) 172.

[13] E.C. Aifantis // *International Journal of Plasticity* **3(3)** (1987) 211.

[14] E.C. Aifantis // *Journal of Engineering Materials and Technology-Transactions of the Asme* **106(4)** (1984) 326.

[15] W.A. Soer, K.E. Aifantis and J.T.M. De Hosson // *Acta Materialia* **53(17)** (2005) 4665.

[16] D.M. Dimiduk, M.D. Uchic and T.A. Parthasarathy // *Acta Materialia* **53(15)** (2005) 4065 and K.S. Ng and A.H.W. Ngan // *Acta Materialia* **56** (2008) 1712.

[17] K.E. Aifantis and A.H.W. Ngan // *Materials Science and Engineering A-Structural Materials Properties Microstructure and Processing* **459(1-2)** (2007) 251.

[18] K.E. Aifantis *et al.* // *Acta Materialia* **54(19)** (2006) 5077.

[19] X. Zhang and K.E. Aifantis, *To be submitted. 2010.*

[20] S. Isozaki, S. Takaki and K. Abiko // *Physica Status Solidi* **A 167** (1998), p. 471.

[21] S. Akarapu, H.M. Zbib and D.F. Bahr // *International Journal of Plasticity* **26(2)** (2010) 239.

[22] W. Wen and J.G. Morris // *Materials Science and Engineering A* **354(1-2)** (2003) 279.

[23] C. Huang *et al.* // *Advanced Engineering Materials* **10(5)** (2008) 434.

[24] P.G. Sanders, J.A. Eastman and J.R. Weertman // *Acta Materialia* **45(10)** (1997) 4019.

[25] I.A. Ovid'ko // *International Materials Reviews* **50(2)** (2005) 65.

[26] K. Lu, L. Lu and S. Suresh // *Science* **324(5925)** (2009) 349.

[27] I.A. Ovid'ko // *Journal of Materials Science* **42(5)** (2007) 1694.

[28] M. Meyers, A. Mishra and D. Benson // *Progress in Materials Science* **51(4)** (2006) 427.

[29] I.A. Ovid'ko and A.G. Sheinerman // *Acta Materialia* **57(7)** (2009) 2217.

[30] I.A. Ovid'ko, A.G. Sheinerman and E.C. Alfantis // *Acta Materialia* **56(12)** (2008) 2718.

[31] J. Schiøtz *et al.* // *Physical Review B* **60** (1999) 11971.